01 Feb 2000

EMI from Cavity Modes of Shielding Enclosures-FDTD Modeling and Measurements

Min Li

Joe Nuebel

James L. Drewniak
Missouri University of Science and Technology, drewniak@mst.edu

Richard E. DuBroff
Missouri University of Science and Technology, red@mst.edu

et. al. For a complete list of authors, see https://scholarsmine.mst.edu/ele_comeng_facwork/1006

Recommended Citation

M. Li et al., "EMI from Cavity Modes of Shielding Enclosures-FDTD Modeling and Measurements," *IEEE Transactions on Electromagnetic Compatibility*, vol. 42, no. 1, pp. 29-38, Institute of Electrical and Electronics Engineers (IEEE), Feb 2000.
The definitive version is available at https://doi.org/10.1109/15.831702

EMI from Cavity Modes of Shielding Enclosures—FDTD Modeling and Measurements

Min Li, Joe Nuebel, *Member, IEEE*, James L. Drewniak, *Member, IEEE*, Richard E. DuBroff, *Senior Member, IEEE*, Todd H. Hubing, *Senior Member, IEEE*, and Thomas P. Van Doren, *Senior Member, IEEE*

***Abstract*—Electromagnetic interference (EMI) from slots and apertures resulting from coupling of interior sources through enclosure cavity modes in a rectangular test enclosure is reported herein. EMI from a specially designed test enclosure with slots or apertures excited by interior sources was studied experimentally and with finite-difference time-domain (FDTD) modeling. The measurements and FDTD modeling agree well. The results indicate that radiation at cavity mode resonances through slots and apertures of nonresonant dimensions can be as significant as the radiation at aperture or slot resonances. The agreement between the FDTD modeling and measurements demonstrates the usefulness of FDTD for investigating aspects of shielding enclosure design such as coupling to slots and apertures and slot interactions.**

***Index Terms*—Cavity-mode resonances, FDTD, enclosure.**

I. Introduction

THE integrity of shielding enclosures for high-speed digital designs is compromised by slots and apertures for heat dissipation, CD-ROMs, input/output (I/O) cable penetration, and plate-covered unused connector ports, among other possibilities. Radiation from slots (the length is much greater than the width) and apertures (the length and width are comparable) in conducting enclosures excited by interior printed circuit board (PCB) level sources is of great concern in meeting the Federal Communications Commission's (FCC) radiated electromagnetic interference (EMI) limits. At frequencies above the fundamental cavity-mode resonance, radiation from enclosures can dominate radiation from I/O cables connecting the high-speed PCB to peripherals. An understanding of energy coupling mechanisms to and from the enclosure as well as an experimentally demonstrated modeling approach is essential in minimizing the EMI and susceptibility risk in a new design.

Considerable work has been done on the admittance of cavity-backed slots [1]–[3] that concentrates on the slot resonances that occur below the resonances of the backing cavity. Extensive efforts—both experimental and numerical—have also been reported on the shielding effectiveness of enclosures at frequencies below cavity-mode resonances [4]–[7]. More recent efforts have studied an analytical formulation for the shielding effectiveness of an empty enclosure with apertures using an equivalent circuit for the shorted waveguide and aperture impedance [8], but only up to the fundamental cavity mode resonance. A calculation of the shielding effectiveness of rectangular enclosures with apertures by a modal expansion technique has also been reported [9]. A means of obtaining the tangential electric fields numerically or experimentally, and applying equivalence principles to estimate the radiation from apertures has been shown [10] as well as the shielding effectiveness of a shielding enclosure with apertures of varying area [11]. A power balance method to estimate Q factors of resonances associated with a shielding enclosure has also been reported [12]. Much of the previous work, however, has focused on an analytical formulation of enclosure and aperture modeling. While analytical approaches can provide insight and direction on enclosure design, incorporating even gross geometric irregularities common in high-speed digital products such as PCB conducting planes as well as the overall loading effects of the electronics are precluded.

The work reported herein details coupling through slots and apertures at cavity mode resonances resulting in EMI as well as new resonances associated with the interaction between the cavity and slot and resonances due to the slots and apertures. EMI, from perforations in a shielding enclosure, was studied experimentally and with finite-difference time-domain (FDTD) modeling. Among the significant results is that EMI at cavity mode resonances through nonresonant slots or apertures can be as significant as that from resonant slots and apertures. Further, the EMI from closely spaced multiple electrically short slots is proportional to the number of slots. Good agreement between the measurements and modeling shows that numerical modeling of enclosure designs can be a useful aid in understanding fundamental coupling physics and in developing EMI design guidelines for enclosures. Lossy materials have also been incorporated into the study and can be used to mimic a distributed PCB loss or in design for reducing the Q of resonances.

The particular aspects of concern for enclosure designs in general were: 1) the EMI coupling mechanism (slot resonances or cavity mode resonances); 2) the relation between EMI and slot length; 3) multiple slot interactions; and, 4) utilizing lossy materials. A test enclosure was then designed with a rectangular interior shape and well-controlled slot parameters to simplify and concentrate on the enclosure study. Measurements and FDTD modeling were both utilized in the study to understand the EMI coupling mechanism, as well as slot interactions in the shielding enclosure.

Manuscript received October 14, 1998; revised October 12, 1999. This work was supported by the University of Missouri-Rolla EMC Consortium.

M. Li was with the University of Missouri-Rolla. She is currently with Lucent Technologies, Engineering Reseach Center, Princeton, NJ 08542 USA.

J. Nuebel is with Sun Microsystems, Palo Alto, CA 94303 USA.

J. L. Drewniak, R. E. DuBroff, T. H. Hubing, and T. P. Van Doren are with the Department of Electrical Engineering, University of Missouri-Rolla, Rolla, MO 65409-0249 USA.

Publisher Item Identifier S 0018-9375(00)02181-5.

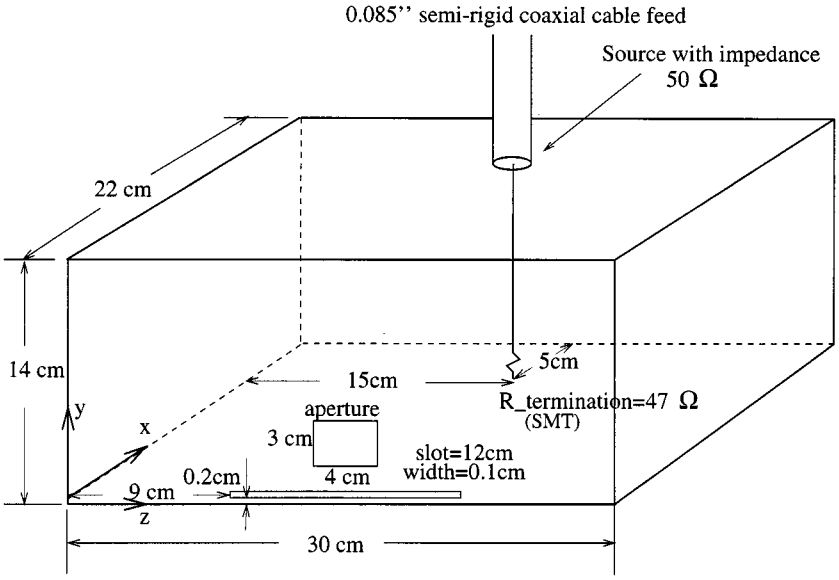

Fig. 1. A rectangular test enclosure.

II. Experimental Configuration and FDTD Modeling

EMI from shielding enclosures was studied using a simple rectangular shielding enclosure. The simple rectangular enclosure accommodated straightforward identification of cavity modes as well as comparison between measurements and FDTD modeling. The geometry of this enclosure is shown in Fig. 1. The enclosure was constructed of five pieces of 0.635-cm-thick aluminum and one plate of 0.05-cm-thick aluminum for the face containing the slot or aperture. The cavity was constructed so that it could easily be disassembled and reassembled for repeatable measurements. The inside dimensions of the enclosure were 22 cm $\times$ 14 cm $\times$ 30 cm. One-inch copper tape with a conductive adhesive was used as an electromagnetic seal along the seams in the interior. The cavity was fed with a 50-Ω coaxial cable probe through a type-N bulkhead connector, which was peripherally bonded to the cavity. Two different methods of excitation were employed. In one case, as shown in Fig. 1, the center conductor of the probe was extended to span the width of the cavity with a 0.16-cm-diameter wire and terminated on the opposite cavity wall with a 1206 package size surface-mount (SMT) nominal 47-Ω resistor soldered to a 1.5 in $\times$ 1.5 in square of conductive adhesive copper tape. This source geometry was employed in order to introduce the loss necessary in the FDTD modeling. In the other case, the center of a 5 cm $\times$ 9 cm copper patch was connected to a 3-cm-long wire extending from the center conductor of the bulkhead connector. The patch was used to mimic the heatsink within a computer server enclosure [13]. The type N bulkhead connector was located at $x = 17$ cm, $y = 14$ cm, $z = 15$ cm. Using an HP4291A impedance analyzer together with the HP16192A SMT test fixture, the SMT resistor in the first excitation method (Fig. 1) was found to have a constant impedance $|Z| = 47\ \Omega$ and a small reactance $|X| < 3\ \Omega$ over the entire frequency range of the measurements.

S-parameters and radiated EMI measurements were also performed in a 3-m anechoic chamber, as shown in Fig. 2. Two-port

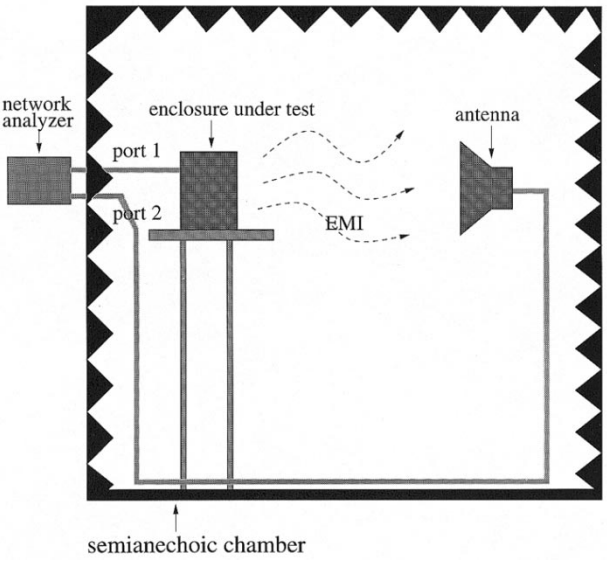

Fig. 2. Experimental setup.

S-parameters were measured with a Wiltron 37247A network analyzer. Port 1 was connected to the interior source in the enclosure under test, and Port 2 was connected to a receiving antenna. For measurements below 1 GHz a log-periodic antenna was used, while for measurements above 1 GHz a horn antenna was used. The network analyzer was placed outside the anechoic room to measure the reflection coefficient $|S_{11}|$ and the transmission coefficient $|S_{21}|$. The power delivered to the enclosure is related to the reflection coefficient as [14]

$$P = \frac{V_s^2}{8Z_0}(1 - |S_{11}|^2) \tag{1}$$

where V_s is the source voltage and Z_0 is the source impedance as well as the characteristic impedance of the coaxial cable. In this particular case, the source voltage is scaled to 1 mV and the source impedance equals the characteristic impedance (50 Ω)

of the coaxial cable connected to ports 1 and 2. The available power is then 2.5 nW. The enclosure and slot resonances can be determined from the frequency dependence of the delivered power.

Far-zone electric field measurements were made with a separation of 3 m between the enclosure and the receiving antenna. The far-zone electric field provides a quantitative measurement of the levels of EMI and is related to the S-parameters by [15]

$$E_{far} = AF \times |S_{21}| \times V_1 \tag{2}$$

where AF is the antenna factor of the receiving antenna and V_1 is the incident voltage at Port 1, which is 0.5 mV for the scaled 1 mV source with 50-Ω source impedance. The enclosure resonances and slot resonances are determined from the delivered power and the far-zone electric field indicates EMI peaks. From the relation between delivered power and far-zone fields, the coupling of EMI from the shielding enclosure can be studied.

The FDTD method was used to model the test enclosure excited by a terminated feed probe. A cell size of 1.0 cm $\times$ 0.5 cm $\times$ 1.0 cm was employed in the FDTD modeling. A finer discretization along the y-direction was used in order to better model the spatial extent of the SMT load resistor. Aluminum plates were modeled with perfectly electrical conductor (PEC) surfaces by setting the tangential electric field to zero on the cavity walls. The wire feed probe was modeled using a thin-wire subcellular algorithm [16], with a radius of 70% of the physical radius [17]. The feed source was modeled by a simple voltage source V_s with 50-Ω resistance incorporated into a single cell at the feed point. The magnetic fields circling the source were modeled in the same fashion as a thin wire to give the cross section of the source with the specified physical dimensions [18]. The resistor was modeled as a lumped element using a subcellular algorithm [19]. The width of the SMT is approximately that of the feed-wire diameter and the physical cross-section dimensions were modeled with the same diameter as that of the feed wire by modifying the magnetic field components circling the SMT in the same fashion as for the source. Thin slots were modeled with the capacitive thin-slot formalism (C-TSF) introduced by Gilbert and Holland [20], as applied to shielded enclosures [17].

The far-zone field was obtained by applying equivalence theory to the numerical FDTD modeling results. Referring to Fig. 3, the FDTD method was used to calculate the electric and magnetic fields on a virtual surface completely surrounding the FDTD model of the enclosure. From the modeled values of the electric and magnetic fields on this surface, equivalent magnetic and electric surface current distributions were determined. The electric and magnetic vector potentials in the frequency domain are related to the electric and magnetic surface current distributions on a virtual surface S' through [21]

$$\vec{A}(\vec{r},\omega) = \frac{\mu_0}{4\pi} \int_{S'} \vec{J}_s(\vec{r}',\omega) \frac{e^{-jk|\vec{r}-\vec{r}'|}}{|\vec{r}-\vec{r}'|}\, ds'(\vec{r}') \tag{3}$$

$$\vec{F}(\vec{r},\omega) = \frac{\epsilon_0}{4\pi} \int_{S'} \vec{M}_s(\vec{r}',\omega) \frac{e^{-jk|\vec{r}-\vec{r}'|}}{|\vec{r}-\vec{r}'|}\, ds'(\vec{r}'). \tag{4}$$

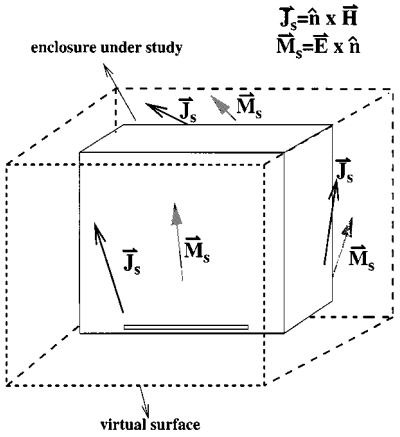

Fig. 3. Application of equivalence theory to calculate the far-zone electric field in the FDTD modeling.

The far-zone electric field components $E_\theta(\vec{r},\omega)$, and $E_\phi(\vec{r},\omega)$ are then

$$E_\theta(\vec{r},\omega) = -j\omega[A_\theta(\vec{r},\omega) + \eta F_\phi(\vec{r},\omega)] \tag{5}$$

$$E_\phi(\vec{r},\omega) = -j\omega[A_\phi(\vec{r},\omega) - \eta F_\theta(\vec{r},\omega)]. \tag{6}$$

Some previous work on near-zone to far-zone transformation implements all of the above equations in the FDTD modeling and directly obtains the far-zone electric field in time domain [22]. In this paper, only (3) and (4) for the electric and magnetic vector potentials are implemented in the FDTD modeling, while the far-zone electric field is obtained in the fast Fourier transform (FFT) process from (5) and (6). As an example, consider one face of the virtual surface shown in Fig. 3. Let the outward normal direction to this face be given by $\hat{n} = \hat{x}$. The electric and magnetic vector potentials are then

$$A_x(\vec{r},t) = 0 \tag{7}$$

$$A_y(\vec{r},t) = \sum_i \frac{\mu_0}{4\pi} \frac{\delta y \delta z}{R_i} \left[-H_z\left(t - \frac{R_i}{c}\right)\right] \tag{8}$$

$$A_z(\vec{r},t) = \sum_i \frac{\mu_0}{4\pi} \frac{\delta y \delta z}{R_i} \left[H_y\left(t - \frac{R_i}{c}\right)\right] \tag{9}$$

$$F_x(\vec{r},t) = 0 \tag{10}$$

$$F_y(\vec{r},t) = \sum_i \frac{\epsilon_0}{4\pi} \frac{\delta y \delta z}{R_i} \left[E_z\left(t - \frac{R_i}{c}\right)\right] \tag{11}$$

$$F_z(\vec{r},t) = \sum_i \frac{\epsilon_0}{4\pi} \frac{\delta y \delta z}{R_i} \left[-E_y\left(t - \frac{R_i}{c}\right)\right] \tag{12}$$

where the summation index i represents an FDTD cell on this surface. R_i is the distance from this FDTD cell to a point having a position vector of $\vec{r}$. Since the values of the electric and magnetic fields appearing within the summation ((7)–(12)) are only

calculated at specific sampling instants, the values of $t - R_i/c$ are rounded up (or down) to the nearest sampling instant. The spatial sampling intervals in the y and z directions are represented by δy and δz, respectively. The contributions to the electric and magnetic vector potentials at a far-zone observation point from all the electric and magnetic surface currents on the six virtual surfaces are then summed.

The far-zone electric field components $E_\theta(\vec{r},\omega)$ and $E_\phi(\vec{r},\omega)$ are then obtained by the application of (5) and (6) and, in the following section, will be compared with the measured values. The virtual surfaces were placed three cells away from the enclosure in the FDTD modeling. Perfectly matched layer (PML) absorbing boundary conditions were employed for the three-dimensional (3-D) FDTD modeling [23]. The PML absorbing layers were four cells away from the conducting planes without a slot and eight cells away from the conducting planes containing or near a slot.

III. FDTD Modeling and Measured Results

Measurements and FDTD modeling were conducted on the rectangular test enclosure with a 12-cm-long and 0.1-cm-wide thin slot, as shown in Fig. 1. The results of delivered power and far-zone electric field are shown in Fig. 4. The frequency range studied was from 0.7 GHz to 1.6 GHz, which included several cavity modes as well as the slot half-wavelength resonance. The agreement between the measurements and modeling is good in both cases. The electric field below 1 GHz was measured with a log-periodic antenna and above 1 GHz with a horn antenna. The cavity-mode resonances and the resonances due to the slot were distinguished by observing the delivered power measurements as the slot length was varied. With the reduction of slot length, the cavity mode resonance frequencies were almost unchanged and the resonances due to the slot disappeared from this frequency range. Since the feed-probe wire was along the y-direction, the y-component of the electric field was excited while the y-component of the magnetic field was suppressed, i.e., only TM_y cavity modes were excited by the probe wire. The cavity-mode resonances, slot resonances, and cavity-slot resonances are shown in Table I. The cavity-slot resonances may be due to reactance tuning, and have been previously denoted cavity-slot modes [24]. The terminated feed probe acting as a matched half-wavelength transmission line caused the broad-band resonance at 1.08 GHz and there is no radiation at this resonance [25]. The frequencies of peaks in the far-zone electric field match the cavity-mode resonance and cavity-slot resonance frequencies. Furthermore, the magnitudes of the peaks at cavity mode resonances are roughly comparable to the magnitudes of the peaks at the slot and cavity-slot mode resonances, as can be seen from Fig. 4(a) and (b). The maximum EMI level in the 0.7–1.6 GHz range occurs for the cavity-slot mode at 1.53 GHz. This EMI level, corresponding to a source voltage of 1 mV, is close to the FCC class B limit.

The slot length was then varied in order to study the EMI effect of slots at frequencies below the half-wavelength slot resonance. Referring again to Fig. 1, various lengths of copper tape were placed over the ends of the slot to reduce the slot length. The slot length was reduced by equal amounts on both ends so

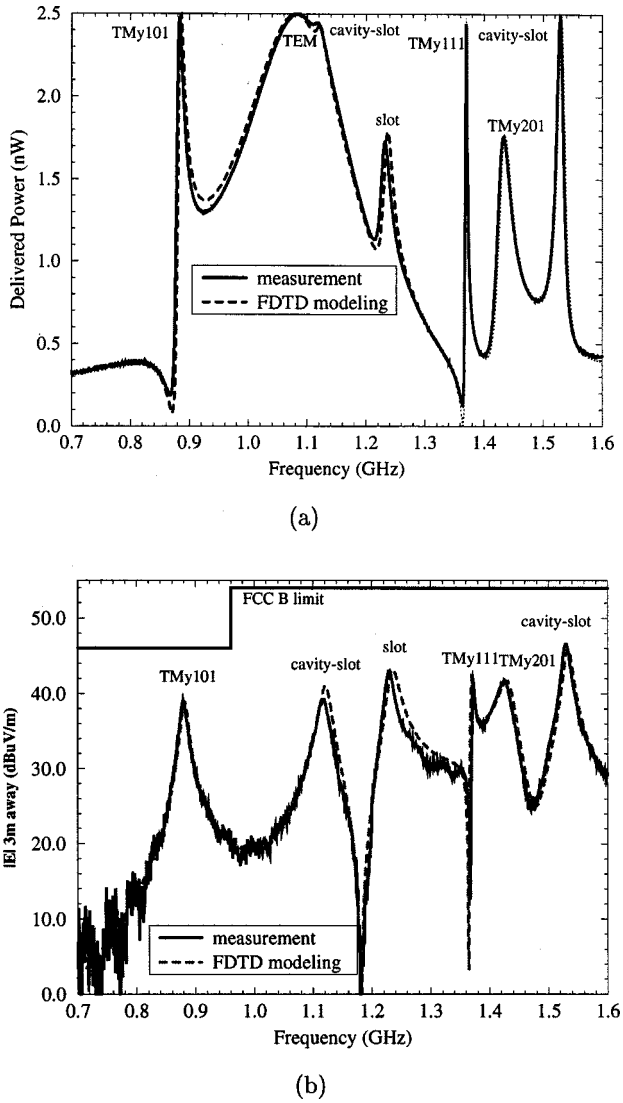

Fig. 4. Measured and modeled results for the test enclosure with a 1-mV source. (a) Delivered power. (b) Electric field at 3 m.

that the center of the effective slot remained in the same position as the copper tape was added and removed. Measurements of the delivered power and electric field at 3 m for slot lengths of 12 cm, 9 cm, and 5 cm are shown in Fig. 5 and agree well with the FDTD modeling results. The peaks labeled A1, A2, B1, B2, C1, and C2 in the electric field at 3-m curve correspond to resonances associated with the slot. With a slot length of 12 cm, these peaks are roughly commensurate with the peaks at the cavity resonance frequencies. When the slot length is reduced, these peaks are not as high as the peaks at the cavity resonance frequencies. Also, these peaks are narrow-band with a high Q factor and, thus, less important to EMI. In short, the dominant peaks in the electric field at 3 m correspond to cavity resonances at frequencies below the half-wavelength resonance of the slot.

Similar sets of measurements were made for the patch source described in the previous section. The physical dimensions of this patch source were chosen to mimic the heatsink in a computer server enclosure. With a 12 cm $\times$ 0.1 cm slot as shown in Fig. 1, the delivered power and far-zone electric field were measured and are shown in Fig. 6. The first resonance at 0.7 GHz is

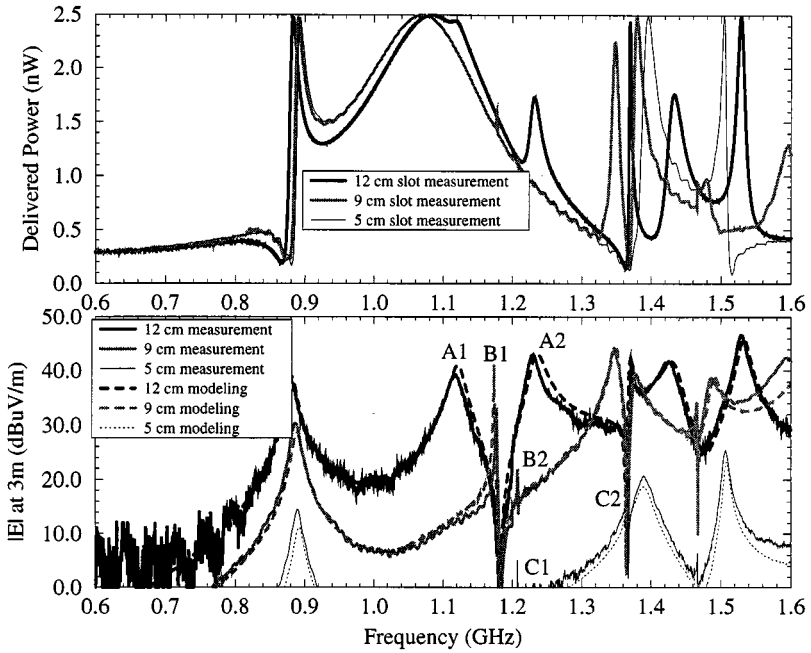

Fig. 5. Measured delivered power and measured and modeled electric field at 3 m for slots of various lengths.

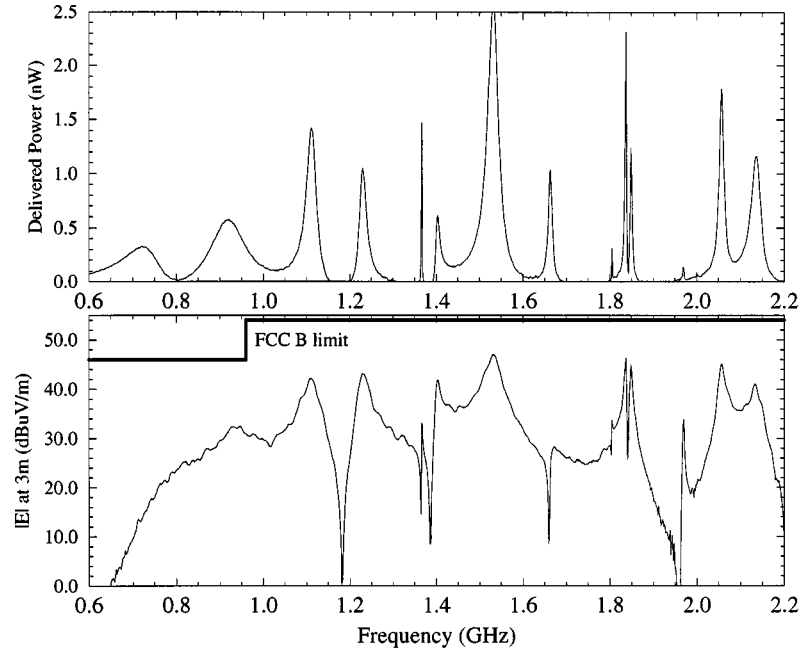

Fig. 6. Measured delivered power and electric field at 3 m for the test enclosure with a 12-cm slot excited by a patch source with $V_s = 1$ mV.

associated with the physical dimensions of the patch and does not appear to contribute significantly to the radiated electric field. Peaks in the delivered power at 0.90, 1.37, 1.41, 1.66, 1.85, 1.96, 2.05, and 2.13 GHz are associated with cavity-mode resonances while peaks at 1.10, 1.24, 1.53, 1.80, and 1.86 GHz can be identified as cavity-slot modes. The frequencies of the first three cavity-slot modes agree with the cavity-slot mode resonance frequencies observed using the previous source (terminated feed probe). At the cavity mode resonance frequencies, the magnitude of the electric field at 3 m varies from approximately 28 dBμ to 45 dBμV/m. At resonances due to the slot, the magnitude of the electric field at 3 m varies from approximately 34 dBμ to 47 dBμV/m.

The electronics in the product enclosures are usually too complicated to be directly modeled with any numerical method. From the measurements on the computer server enclosure with electronics, the loading effect of electronics is appreciable [26]. Lossy materials may be used in the enclosure to mimic the loading effect of the electronics for FDTD modeling purposes [26] and the effect of conductive lossy materials was also studied herein. Two layers of Milliken conductive 110 $\Omega/\square$ lossy material were placed on the $x = 22$ cm interior plane.

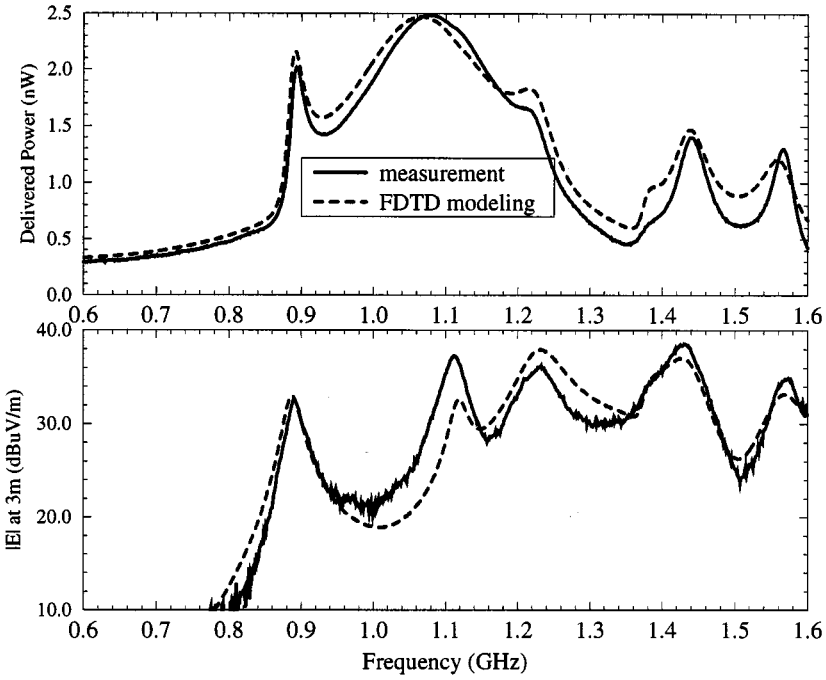

Fig. 7. Measured and modeled delivered power and electric field at 3 m for the test enclosure with a 110 Ω/□ lossy material on one wall.

TABLE I
RESONANCES ASSOCIATED WITH THE SHIELDING ENCLOSURE SHOWN IN FIG. 1

Modes	Frequency (GHz)
TM_y101	0.89
TM_y111	1.37
TM_y201	1.43
slot	1.24
cavity-slot	1.10
cavity-slot	1.53

TABLE II
RESONANCES ASSOCIATED WITH THE SHIELDING ENCLOSURE LOADED WITH LOSSY MATERIAL

Modes	Frequency (GHz)
TM_y101	0.89
TM_y111	1.36
TM_y201	1.44
cavity-slot	1.20
cavity-slot	1.53

The thickness for each layer was 0.4 cm, and the conductivity of the lossy material used in the FDTD modeling was $\sigma = (1/R_{\square}d) = 0.0227$ S/cm. The lossy material was simply modeled by a one-cell layer of conducting material with conductivity $\sigma = 0.0227$ S/cm. For the electric field components inside the conducting layer, the conductivity $\sigma = 0.0227$ S/cm was employed, while the conductivity $\sigma = (0.0227/2)$ S/cm was employed for the components on the interface of the conducting layer and free-space [27].

The measured and modeled delivered power and electric field strength at 3 m are shown in Fig. 7, with the lossy material on the interior face $x = 22$ cm. The agreement between measurements and FDTD modeling is generally good. The effect of the lossy material in decreasing the Q's of resonances is evident in the delivered power and reflected in the reduced radiation in the 3-m electric field. The results in Figs. 4 and 7 can be compared at the resonances indicated in Tables I and II. However, a resonance and a corresponding increase in radiation were observed at 1.20 GHz, where the two resonances due to the slot at 1.10 GHz and 1.24 GHz for the situation without the lossy material may have shifted and broadened to produce a resonance at 1.20 GHz. Overall, a lossy material can be easily incorporated in the FDTD modeling, and may be used to mimic the electronics in the initial shielding enclosure design stage. For example, a conducting plane with a lossy dielectric on it can be used to approximate a PCB (that has entire power or ground planes) with electronics for FDTD modeling of enclosure designs.

Multiple slots were also investigated to study EMI at cavity-mode resonances. Three configurations of twin slots were employed, as shown in Fig. 8. In configuration 1, two slots on different cavity faces were studied. In configuration 2, two parallel slots on the same face were employed with a distance of 0.9-cm edge-to-edge spacing. In configuration 3, two slots end-to-end with a distance of 1 cm between the near ends were studied. All the slot lengths were 12 cm with widths of 0.1 cm and the terminated feed probe source was

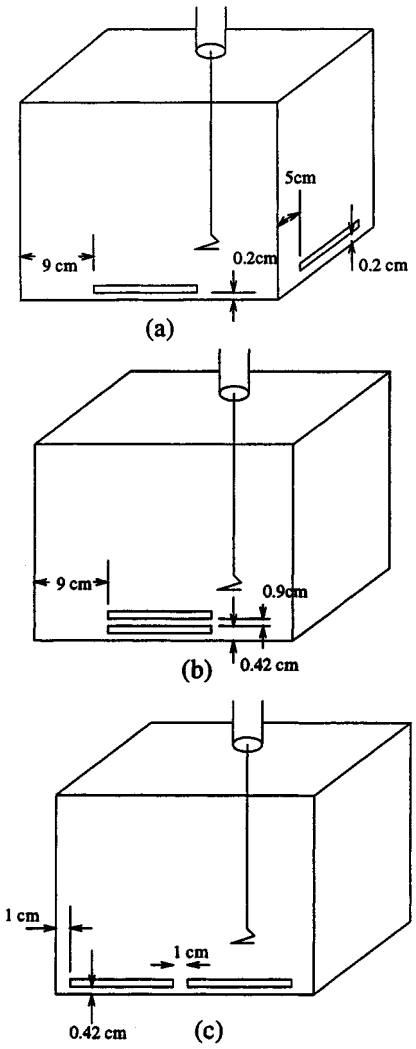

Fig. 8. The configurations for multiple slots. (a) Configuration 1—two slots on different enclosure faces. (b) Configuration 2—two slots side-by-side. (c) Configuration 3—two slots end-to-end.

employed as the cavity excitation. The measured and modeled delivered power and far-zone fields are shown in Fig. 9. Above 1 GHz, the agreement is good for all three configurations. Unfortunately, calibration data for the horn antenna used in these measurements was not available for frequencies below 1 GHz. Therefore, measurements at the TM_y101 resonance frequency (0.885 GHz) are relatively unreliable when compared to measurements above 1 GHz.

The radiation at cavity mode resonances is comparable to the radiation at resonances due to the slot. A comparison of Fig. 9(b) and (c) with Fig. 4(b) suggests that the additional slot in the configuration used in Fig. 9 does not yield more than a few decibels change in either the delivered power or in the far-zone electric field. In this case, the slot is not electrically small over the given frequency range. Comparing Fig. 9(a) with (b) and (c) shows that the presence of two slots on adjacent cavity walls significantly alters the pattern of resonance frequencies.

Reducing the length of each slot from 12 to 5 cm raises the half-wavelength resonance frequency of each slot to approximately 3 GHz—well above the frequency range of the measurements presented here. Therefore, a set of measurements and FDTD modeling was made using two 5-cm-long slots similar to the configurations shown in Fig. 8. Copper tape was used to reduce the 12- to 5-cm slots. In configuration 1, the left end of the 5-cm slot in the $x = 0$ face was 16 cm from the $x = 0, z = 0$ edge and the left end of the 5-cm slot in the $z = 30$ cm face was 5 cm from the $x = 0, z = 30$ cm edge. In configuration 2, the left end of the two side-by-side 5-cm slots were 12 cm from the $x = 0, z = 0$ edge. In configuration 3, the left end of the slots was 9 cm from the $x = 0, z = 0$ edge and the spacing between the near ends of these two slots was 1 cm.

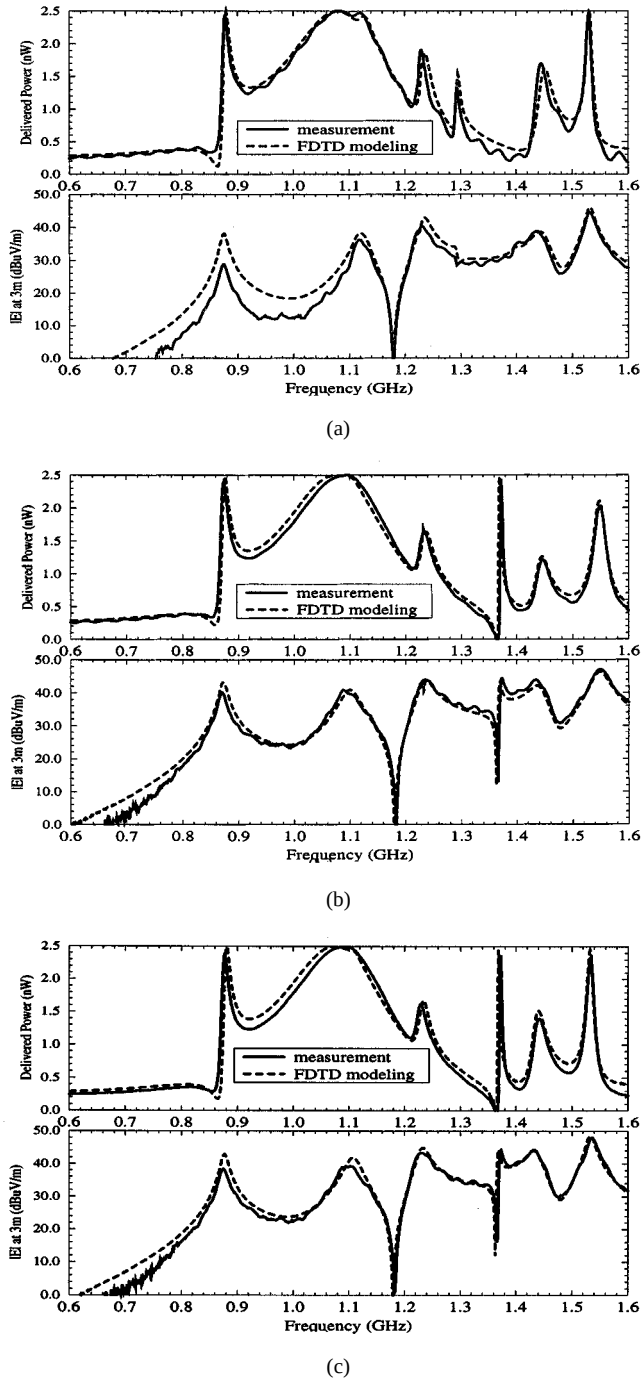

Fig. 9. Measured and modeled delivered power and electric field at 3 m for multiple 12 cm slots. (a) Configuration 1. (b) Configuration 2. (c) Configuration 3.

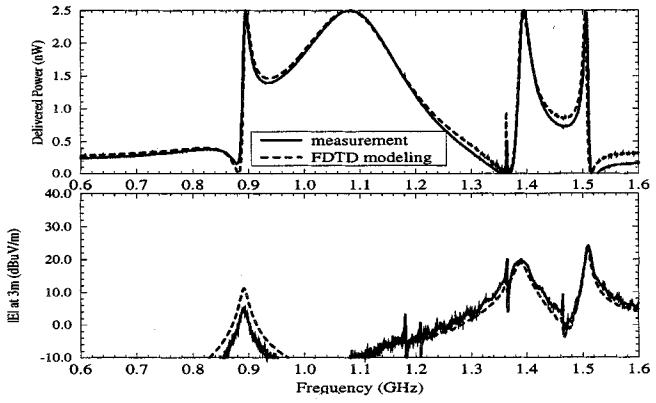

(a)

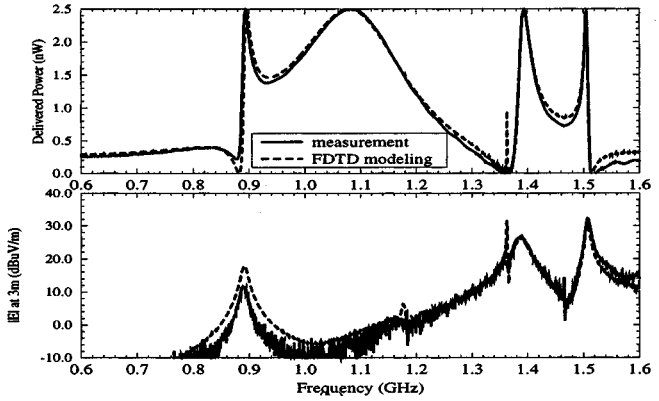

(b)

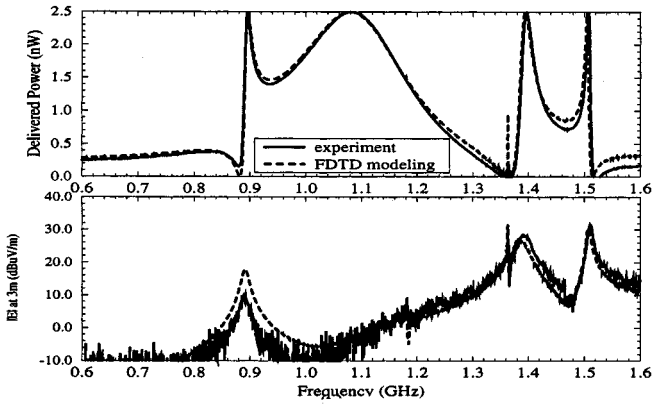

(c)

Fig. 10. Measured and modeled electric field at 3 m for multiple 5-cm-long slots. (a) Configuration 1. (b) Configuration 2. (c) Configuration 3.

Measurement and FDTD modeling results, consisting of the delivered power and the electric field at 3 m for each configuration, are shown in Fig. 10. The cavity-mode resonances in this frequency range can be identified and are listed in Table III. The electric field plots show for each of the three configurations that these cavity resonances are associated with significant peaks in the radiated EMI level. For each configuration, there is also a peak in the electric field at 3 m at a frequency of approximately 1.36 GHz. This peak represents a cavity-slot resonance and is unlikely to be associated with high levels of EMI when the enclosure is excited by active digital electronics since this peak has a very narrow bandwidth. Further, incorporating the effects of loss will appreciably damp this high-Q resonance. Much smaller cavity-slot mode peaks occur at approximately 1.18 GHz for all configurations and at 1.21 GHz for the configuration of slots on adjacent cavity walls (configuration 1). Again these peaks have narrow bandwidths in addition to relatively small amplitudes and would therefore be even less likely to be associated with high levels of EMI. In comparing the radiated electric field from a single 5-cm slot with that from a pair of closely spaced 5-cm slots located in the same wall of the cavity, the double slot configurations were approximately 6 dB higher. The EMI varying with the number of perforations N has been demonstrated for closely spaced electrically small apertures used for airflow [28], even for a relatively large number of apertures. The preliminary results from the current study, as well as from further FDTD modeling, indicate that closely spaced electrically short slots may behave similarly, i.e., that EMI varies as the number N of slots. However, for very closely-spaced parallel slots this is not the case [29].

TABLE III
RESONANCES ASSOCIATED WITH THE SHIELDING ENCLOSURE WITH 5-cm SLOTS

Modes	Frequency (GHz)
TM_y101	0.885
TM_y111	1.4
TM_y201	1.5
cavity-slot	1.18
cavity-slot	1.36

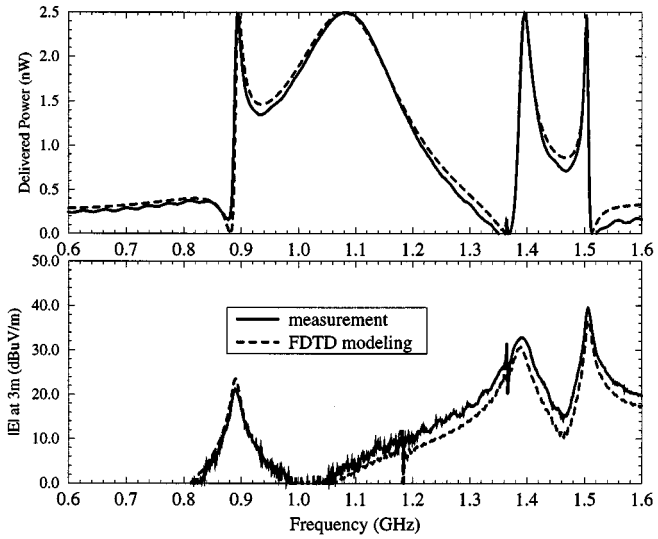

Fig. 11. The measured and modeled delivered power and electric field strength 3 m away through a 3 cm × 4 cm aperture in test enclosure.

Radiation from an aperture was also considered. In this case, a rectangular aperture measuring 3 cm × 4 cm and centered at $y = 5.5$ cm, $z = 15$ cm was cut into the front wall of the cavity, as shown in Fig. 1. In applying the FDTD modeling for this case, the result of electric field at 3 m using the 1.0 cm × 0.5 cm ×

1.0 cm cell size (24 cells in the aperture) was generally 5 dB below the measured result. Then the computational cell size was reduced to 0.5 cm $\times$ 0.5 cm $\times$ 0.5 cm in order to increase the number of FDTD cells modeling the aperture to 48 cells. An improvement of 3 dB was obtained. The measured and FDTD modeling results of both the delivered power and the electric field at 3 m are shown in Fig. 11. The change of the cell size had no significant effect on the FDTD modeling of the delivered power since the power radiated from the aperture was only a small fraction of the total delivered power. The three large, broad peaks in the far zone electric field intensity correspond to cavity-mode resonances at 0.885, 1.4, and 1.5 GHz. Narrow bandwidth peaks occur at 1.18 and 1.36 GHz are associated with the presence of the aperture. Nevertheless, the highest frequency (1.6 GHz) in this measurement is well below the first aperture resonance.

IV. Summary and Conclusion

EMI from slots and apertures in shielding enclosures was investigated with measurements and FDTD modeling. A simple rectangular test enclosure excited with an interior terminated feed-probe source was used to study EMI from a single slot and aperture as well as multiple slots, both electrically short and of resonant dimensions. In general, the agreement between the measurements and modeling was good for both the delivered power and the electric field at 3 m. In the frequency range where slots are near a half-wavelength, the EMI from cavity-mode resonances is comparable to that from the slot resonances and the cavity-slot mode resonances. For slots shorter than a half-wavelength, the EMI from cavity mode resonances dominates, though there are a few narrow bands of increased EMI due to the cavity-slot resonances. These cases are very narrow-band and unlikely to cause serious EMI problems, particularly since loading will decrease the Q of these resonances considerably. The radiation from a small aperture is similar to that of a short slot, as long as the frequency is below the aperture resonance.

The effect of conductive lossy materials on radiated EMI resulting from cavity modes and slot resonances, as well as FDTD modeling of these materials in an enclosure, were studied. The lossy material damped high-Q cavity resonances. In FDTD modeling, the uniform lossy material can be used to approximate the loss associated with the functioning electronics. For example, a conducting plane covered with the lossy material can approximate a multilayer PCB with at least one entire plane, e.g., power or ground. In addition to serving as an approximation to the loss on the PCB, the lossy material also serves to provide loss in the FDTD modeling so that more general and realistic source geometries can be modeled (such as a driven heatsink) without the need to build loss into the excitation as with the resistively terminated wire probe.

Multiple slots were also investigated. As in the case of single slots and apertures, significant EMI resulted at cavity-mode resonances. The radiation from the combination of two closely spaced slots of appreciable electrical length was not the sum of the radiation from the individual slots. By contrast, the radiation from two closely spaced short slots in the same face, whether side-by-side or end-to-end, is approximately 6 dB higher than the radiation for only one of the slots.

A terminated feed probe or a patch driven against the enclosure were employed as the interior source in this study. The utility of the terminated wire probe was for ease of modeling, i.e., an FDTD subcellular algorithm exists for a thin wire and the resistive termination provides loss for the FDTD time-marching algorithm. However, EMI sources at the PCB level in a functional enclosure that excite the cavity still remain largely unknown. Structures that protrude above the board such as heatsinks are known PCB level structures that excite the enclosure. Realistic source models for the integrated circuit (IC) packages that couple to the heatsinks, however, are necessary in the future to provide absolute EMI levels for a given enclosure geometry and PCB level sources. Presently, FDTD modeling is best suited for understanding fundamental physics and coupling paths as well as addressing relative questions, for example, the EMI reduction for various screw spacings in an enclosure comparing EMI gasketing alternatives or EMI for various air-flow aperture array designs.

Acknowledgment

The authors would like to thank Sun Microsystems for making their 3-m chamber available for radiated EMI measurements.

References

[1] J. Galejs, "Admittance of a rectangular slot which is backed by a rectangular cavity," *IEEE Trans. Antennas Propagat.*, vol. AP-11, pp. 119–126, Mar. 1963.

[2] C. R. Cockrell, "The input admittance of the rectangular cavity-backed slot antenna," *IEEE Trans. Antennas Propagat.*, vol. AP-24, pp. 288–294, May 1976.

[3] S. A. Long, "Experimental study of the impedance of cavity-backed slot antennas," *IEEE Trans. Antennas Propagat.*, vol. AP-23, pp. 1–7, Jan. 1975.

[4] S. Daijavad and B. J. Rubin, "Modeling common-mode radiation of 3-D structures," *IEEE Trans. Electromagn. Compat.*, vol. 34, pp. 57–61, Feb. 1992.

[5] S. Hashemi-Yeganeh and C. Birtcher, "Theoretical and experimental studies of cavity-backed slot antenna excited by a narrow strip," *IEEE Trans. Antennas Propagat.*, vol. 41, pp. 236–241, Feb. 1993.

[6] J. Y. Lee, T. S. Horng, and N. G. Alexopoulos, "Analysis of cavity-backed aperture antennas with a dielectric overlay," *IEEE Trans. Antennas Propagat.*, vol. 42, pp. 1556–1561, Nov. 1994.

[7] H. A. Mendez, "Shielding theory of enclosures with apertures," *IEEE Trans. Electromagn. Compat.*, vol. EMC-20, pp. 296–305, May 1978.

[8] M. P. Robinson, T. M. Benson, C. Christopoulos, J. F. Dawson, M. D. Ganley, A. C. Marvin, S. J. Porter, and D. W. P. Thomas, "Analytical formulation for the shielding effectiveness of enclosures with apertures," *IEEE Trans. Electromagn. Compat.*, vol. 40, pp. 240–248, Aug. 1998.

[9] W. Wallyn, F. Olyslager, E. Laermans, D. D. Zutter, R. D. Smedt, and N. Lietaert, "Fast evaluation of the shielding effectiveness of rectangular shielding enclosures," in *Proc. IEEE Electromagn. Compat. Symp.*, Denver, CO, Aug. 1998.

[10] G. Cerri, R. D. Leo, and V. M. Primiani, "Theoretical and experimental evaluation of the electromagnetic radiation from apertures in shielded enclosure," *IEEE Trans. Electromagn. Compat.*, vol. 34, pp. 423–432, Nov. 1992.

[11] H. Y. Chen, I.-Y. Tarn, and Y.-J. He, "NEMP fields in side a metallic enclosure with an aperture in one wall," *IEEE Trans. Electromagn. Compat.*, vol. 37, pp. 99–105, Feb. 1995.

[12] D. A. Hill, M. T. Ma, A. R. Ondrejka, B. F. Riddle, M. L. Crawford, and R. T. Johnk, "Aperture excitation of electrically large, lossy cavities," *IEEE Trans. Electromagn. Compat.*, vol. 36, pp. 169–177, Aug. 1994.

[13] S. Radu, Y. Ji, J. Nuebel, J. L. Drewniak, T. P. Van Doren, and T. H. Hubing, "Identifying an EMI source and coupling path in a computer system with submodule testing," in *Proc. IEEE Electromagn. Compat. Symp.*, Austin, TX, Aug. 1997, pp. 165–170.
[14] D. M. Pozar, *Microwave Engineering*. Reading, MA: Addison-Wesley, 1990.
[15] D. Morgan, *A Handbook for Testing and Measurement*. Stevenage, U.K.: Peter Peregrinus, 1994.
[16] A. Taflove, *Advances in Computational Electrodynamics: The Finite-Difference Time-Domain Method*. Boston, MA: Artech House, 1998.
[17] M. Li, K.-P. Ma, J. L. Drewniak, T. H. Hubing, and T. P. Van Doren, "Numerical and experimental corroboration of an FDTD thin-slot model for slots near corners of shielding enclosures," *IEEE Trans. Electromagn. Compat.*, vol. 39, pp. 225–232, Aug. 1997.
[18] D. M. Hockanson, J. L. Drewniak, T. H. Hubing, and T. P. Van Doren, "FDTD modeling of common-mode radiation from cables," *IEEE Trans. Electromagn. Compat.*, vol. 38, pp. 376–387, Aug. 1996.
[19] Y.-S. Tsuei, A. C. Cangellaris, and J. L. Prince, "Rigorous electromagnetic modeling of chi-to-package (first-level) interconnections," *IEEE Trans. Components Hybrids Manuf. Technol.*, vol. 16, pp. 876–882, Dec. 1993.
[20] J. Gilbert and R. Holland, "Implementation of the thin-slot formalism in the finite-difference EMP code THREDII," *IEEE Trans. Nucl. Sci.*, vol. NS-28, pp. 4269–4274, Dec. 1981.
[21] C. A. Balanis, *Advanced Engineering Electromagnetics*. New York: Wiley, 1989.
[22] R. J. Luebbers, K. S. Kunz, M. Schneider, and F. Hunsberger, "A finite-difference time-domain near zone to far zone transformation," *IEEE Trans. Antennas Propagat.*, vol. 39, pp. 429–433, Apr. 1991.
[23] J. P. Berenger, "Perfectly matched layer for the absorption of electromagnetic waves," *J. Comput. Phys.*, vol. 114, pp. 185–200, Oct. 1994.
[24] C. H. Liang and D. K. Cheng, "Electromagnetic fields coupled into a cavity with a slot-aperture under resonant conditions," *IEEE Trans. Antennas Propagat.*, vol. AP-30, pp. 664–672, July 1982.
[25] M. Li, "Investigation of electromagnetic interference through slots in shielding enclosures: Finite-difference time-domain simulations and experiments," M.S., Univ. Missouri-Rolla, Rolla, MO, 1996.
[26] M. Li, S. Radu, J. L. Drewniak, T. H. Hubing, T. P. VanDoren, and R. E. DuBroff, "EMI vfom shielding enclosures," Electromagn. Compat. Lab., Univ. Missouri-Rolla, Tech. Rep. TR98-1-029, 1998.
[27] D. M. Hockanson, "The finite-difference time-domain method and applications in electromagnetic compatibility," M.S., Univ. Missouri-Rolla, Rolla, MO, 1994.
[28] M. Li, S. Radu, J. Nuebel, J. L. Drewniak, T. H. Hubing, and T. P. VanDoren, "Design of airflow aperture arrays in shielding enclosures," in *Proc. IEEE Electromagn. Compat. Symp.*, Denver, CO, Aug. 1998, pp. 1059–1063.
[29] M. Li, "Modeling and design of shielding enclosures for EMI mitigation—Experiments and finite -difference time-domain and method of moments modeling," Ph.D., Univ. Missouri-Rolla, Rolla, MO, 1999.

Min Li was born in China in 1968. She received the B.S. (honors) and M.S. (honors) degrees in physics from Fudan University, Shanghai, China, in 1990 and 1993, respectively, and the M.S. and Ph.D. degrees in electrical engineering from the University of Missouri-Rolla, in 1996 and 1999, respectively.

Since 1995, she has studied and worked in the EMC Laboratory at the University of Missouri-Rolla. Her research interests include numerical and experimental study of electromagnetic compatibility problems. She is currently with Lucent Technologies.

Dr. Li has been supported in her research and education by a Dean's Fellowship and Assistantship. She is the winner of the 1998 IEEE EMC Society President Memory Award.

Joe Nuebel (M'95) is currently a Staff Electromagnetic Compatibility (EMC) Engineer at Sun Microsystems, Palo Alto, CA. For over 15 years he has been working in the field of EMC. His background also includes immunity, safety, and network equipment building systems (NEBS) testing for Telco. He also initiated university research at Sun in the area of EMC to assist in determining possible future EMC design concepts.

James L. Drewniak (S'85–M'90) received the B.S. (highest honors), M.S., and Ph.D. degrees in electrical engineering all from the University of Illinois, Urbana-Champaign, in 1985, 1987, and 1991, respectively.

In 1991, he joined the Electrical Engineering Department at the University of Missouri-Rolla, where he is part of the Electromagnetic Compatibility Laboratory. His research interests include the development and application of numerical methods for investigating electromagnetic compatibility problems, packaging effects, and antenna analysis, as well as experimental studies in electromagnetic compatibility and antennas.

Richard E. DuBroff (S'74–M'77–SM'84) received the B.S.E.E. degree from Rensselaer Polytechnic Institute, Troy, NY, in 1970, and the M.S. and Ph.D. degrees in electrical engineering from the University of Illinois at Urbana-Champaign, in 1972 and 1976, respectively.

From 1976 to 1978, he held a postdoctoral position in the Ionosphere Radio Laboratory, University of Illinois, Urbana-Champaign, and worked on backscatter inversion of ionospheric electron density profiles. From 1978 to 1984 he was employed as a Research Engineer in the geophysics branch of Phillips Petroleum (Bartlesville, OK). Since 1984 he has been affiliated with the University of Missouri-Rolla and is currently a Professor in the Department of Electrical and Computer Engineering there.

Todd H. Hubing (S'82–M'82–SM'93) received the B.S.E.E. degree from the Massachusetts Institute of Technology, Cambridge, the M.S.E.E. degree from Purdue University, West Lafayette, IN, and the Ph.D. degree in electrical engineering from North Carolina State University, Raleigh, NC, in 1988, respectively.

He is currently a Professor of electrical engineering at the University of Missouri-Rolla (UMR) and a member of the principal faculty in the UMR Electromagnetic Compatibility Laboratory. Prior to joining the faculty at the University of Missouri-Rolla in 1989, he was an Electromagnetic Compatibility Engineer at IBM, Research Triangle Park, NC. He has authored or presented more than 70 technical papers, presentations, and reports on electromagnetic modeling and electromagnetic compatibility-related subjects. He also writes the satirical "Chapter Chatter" column for the *IEEE EMC Society Newsletter*. Since joining the UMR, the focus of his research has been measuring and modeling sources of electromagnetic interference.

Dr. Hubing is on the Board of Directors for the IEEE EMC Society.

Thomas P. Van Doren (S'60–M'69–SM'96) received the B.S., M.S., and Ph.D. degrees from the University of Missouri-Rolla in 1962, 1963, and 1969, respectively.

From 1963 to 1965, he served as an Officer in the U.S. Army Security Agency. From 1965 to 1967 he was a Microwave Engineer with Collins Radio Company, Dallas, TX. Since 1967 he has been a member of the electrical engineering faculty at the University of Missouri-Rolla, where he is currently a Professor. His research interests concern developing circuit layout, grounding, and shielding techniques to improve electromagnetic compatibility. He has taught short courses on electromagnetic compatibility to over 10 000 engineers and technicians representing 200 corporations.

Dr. Van Doren received the IEEE EMC Society Richard R. Stoddard Award for his contributions to electromagnetic compatibility research and education in 1995. He is a Registered Professional Engineer in the state of Missouri and a member of Eta Kappa Nu, Tau Beta Pi, and Phi Kappa Phi.